DEVELOPMENT OF AN ELECTRICAL IMPEDANCE TOMOGRAPHY SYSTEM: DATA COLLECTION AND RECONSTRUCTION ALGORITHM

G. A. Kyriacou*, P. M. Bonovas,* C. S. Koukourlis* and J. N. Sahalos+

* Department of Electrical and Computer Engineering, Demokritos University of Thrace
GR-67100, Xanthi, GREECE. Fax: +30-541-27264
E-mail: gkyriac@demokritos.cc.duth.gr
+ Department of Physics, Aristotle University of Thessaloniki
GR-54006, Thessaloniki, GREECE

Abstract

A detailed step-by-step procedure for the development of an Electrical Impedance Tomography (EIT) system is presented. This is identified into three major tests: the "computer", the "laboratory or in-vitro" and the "clinical or in-vivo" with an increasing difficulty. This work deals with the first two of them. First the EIT basic principles are reviewed and later both the measurements - data collection and reconstruction algorithm procedures are explained. The development of resistive network and the tank laboratory phantom as well as the comparison of the measured and calculated results is then considered. Finally, reconstructed images from both laboratory phantoms are presented and compared against the target models.

1. INTRODUCTION

The Electrical Impedance Tomography (EIT) is a new imaging modality aiming at the reconstruction of an object's conductivity or permittivity distribution. There are a lot of possible applications but the most promising are those in medicine [1] and geophysical prospecting (including archeology), e.g. [2]. All these applications share the same reconstruction algorithm and most of the data collection system, with the exception of the electrodes configuration. This paper will be restricted to the medical applications, since they are of particular interest.

EIT medical imaging is established on the fact that biological tissues can be recognized from their conductivity (σ) or permittivity (ε). Moreover, the tissue electrical properties vary according to its state of health as well as during physiological organs functioning. It is then evident that EIT can be used for medical diagnosis and dynamic events monitoring. The attractive features of EIT that make it appropriate for medical applications is its non-ionizing and non-invasive nature, along with the low cost and the portability of the resulting instrument. Also, the safety requirements are established by keeping the injected current level below the 10mA-rms (preferably around 5mA) according to international regulations, e.g. [3]. This makes EIT appropriate for continuous (24 hours based) patient

monitoring. The main disadvantage of EIT is in general its low resolution. However, its performance on soft tissue imaging (lung, kidney, etc) is considered satisfactory, especially when compared to other established techniques (x-rays computed tomography or ultrasound) resolution on these soft tissues.

An EIT imaging system consists of its data collection-measurement sub-system and its reconstruction algorithm. Our research team has extensively studied and contributed to both fields, e.g. [5-6], [10-13] and the references there in. Two experimental systems are developed and checked so far and another one is under development.

The purpose of this paper is to clearly identify a step-by-step development procedure of an EIT system. First the basic EIT principles are reviewed along with the basic assumptions involved. The development procedure is then defined in three major steps. In turn the data collection hardware and the reconstruction algorithm employed in our last system are described. Finally, reconstructed images from computer simulations and laboratory phantoms are presented. The open problems including the ones under consideration as well as the ones remaining for further investigation are also discussed. Our ambition for this paper is to serve as a guide for any one whom would like to start developing an EIT system.

2. PRINCIPLES OF EIT

In order of EIT to acquire the necessary data a number of electrical measurements are performed on the body of interest. First, an array of equi-spaced electrodes is attached on the surface of the body. A subset of them, called driven electrodes, is used to inject a low frequency (usually between 10 and 100kHz) sinusoidal current pattern with an rms amplitude less than 10 mA (preferably around 5 mA) for safety reasons. The voltage developed on each one of the remaining electrodes, called sensing electrodes, is then measured with respect to a reference electrode. Depending on the system hardware and due to the high common mode voltage between the sensing electrodes it may be preferable to measure the voltage differences on each electrode pair instead of measuring with respect to a reference electrode. The frequency of the injected current must be higher than about 10 kHz to avoid interference from the internal bioelectric sources. Also, frequencies lower than 10 Hz are absolutely prohibited, since they can cause electrolysis or ion migration phenomena, [4].

The above-described measurements are repeated for every possible subset of driven electrodes. With the analogy to the classical tomography terminology, the measurement

process for each specific active electrodes subset is called a "projection angle". In order to reconstruct the object's internal conductivity distribution a calculated data set similar to the measured one is required. For this purpose an initial-starting conductivity distribution is assumed within a computer model, which also includes the electrodes. The calculation procedure then mimics the measurements. Namely, identical current patterns are injected through the same electrodes and the forward problem (Laplace equation) is solved to estimate the corresponding voltage differences. The aim of the reconstruction algorithm is to use (or backproject) the differences between the measured and calculated data in order to update the assumed conductivity distribution. The resulting image is by no means the final one, since the conductivity imaging is a non-linear inverse electromagnetic problem, as it will be explained latter. What we get is just a better approximation to be updated-improved during the next iteration. Namely, keeping the same measured data the calculation procedure is repeated but solving the forward problem for the recently updated conductivity distribution. This is in turn carried-on until the differences (mean squared error) between the measured and calculated data set becomes comparable to the unavoidable measurements error tolerance.

It is important to note here some of the principal assumptions currently considered in EIT. The first one is that a "Quasistatic condition" is valid. Namely, that even though measurements are carried out using an AC-current injection, the calculations can be done at DC. In other words, the forward problem is reduced to the solution of a Laplace (instead of a wave or Helmholtz) equation. This is justified by the fact that the dimensions of the body (of the order of 1 m) are quite smaller than the injected current wavelength (for f=100 kHz it is λ=3 km). This means that the propagation phenomena are negligible or equivalently that the injected current varies in synchronism with time all over the body. The second assumption is that the conduction current ($\vec{J}_d = \sigma\vec{E}, \vec{E} =$ the electric field intensity) is dominant, while the displacement current ($J_d = \partial(\varepsilon\vec{E})\partial t = j\omega\varepsilon\vec{E}$), with $\omega = 2\pi f$) is negligible at low frequencies. Simulations carried out in our previous work [7, p.5-11], show that for the human body materials (tissues) the error of this assumption is less than 0.01% for frequencies upto 1MHz. A consequence of this fact is that the tissue impedance can be treated as purely real upto about 1 MHz. Moreover, the magnetic field effects can be neglected upto about 10 MHz, [5, p.172], since the biological tissues are non-magnetic ($\mu = \mu_o = 4\pi\cdot10^{-7}$ H/m = air permeability). Thus the electric ($\vec{E}$) and magnetic ($\vec{H}$) field intensities are related through the factor $j\omega\mu_o$, which is negligible for frequencies less than

10 MHz. Taking the above into account, the Maxwell equations for the problem of low frequency current injection are reduced to two generalized Laplace (or Poisson) equations, [6, p.17], as:

$$\overline{\nabla} \cdot \left(\varepsilon \overline{\nabla} V\right) = -\rho \tag{1a}$$

$$\overline{\nabla} \cdot \left(\sigma \overline{\nabla} V\right) = \partial\rho / \partial t \tag{1b}$$

where ρ is the internal charge density.

A third assumption is that there are no internal bioelectric sources at the frequency of the applied current. This means that in Eq.(1) it is $\rho = 0$ and the injected current is included through the boundary conditions.

Another important issue is whether the EIT reconstruction can be handled as a 2- or 3-dimensional imaging. A 2-dimensional approach is used in the classical imaging techniques like the x-rays CT. However, the electric current cannot be constrained to flow in a plane, but it is deeply spread above and below the active electrodes plane. Thus, the conductivity reconstruction is in fact a strictly 3-dimensional problem. Moreover, the current streamlines (as well as the voltage equipotential lines) depend on the unknown conductivity distribution. This fact explains the non-linearity of the problem. Also, the current streamlines are more dense near the active electrodes spreading out as we move away from it. Thus, EIT is more sensitive to conductivity variations near the active electrodes, which can only be placed on the object's surface. In turn this effect leads to an ill-conditioned inverse problem. Taking these difficulties into account it was decided by the first investigators of the field to be restricted to the 2-dimensional imaging. But now it is well understood that the investigation must move toward the 3-dimensional reconstruction. It was also observed [7, chapt.6] that 3-D imaging will make calculations more compatible with measurements and this will reduce the ill-conditioning effects.

3. GENERAL EIT SYSTEM DEVELOPMENT PROCEDURE

The research subject of EIT like any other imaging technique can be discriminated into three fields: i) The reconstruction algorithm (software), ii) the Data Collection (hardware) and iii)the medical applications of the method. Based on this, the step-by-step development procedure is established in an order of increasing difficulty. These stages are identified as follows:

a) *Computer Test* This stage aim at the reconstruction of images from "computer phantoms" and its main purpose is to validate the reconstruction algorithm itself. The

target conductivity distribution is simulated using a computer model (phantom) and the Laplace equation is repeatedly solved in order to acquire a data-set labeled "measurements". These data are then used by the reconstruction algorithm, which starts from an assumed homogeneous distribution. This is an imaging with "perfect data" since, the measured data set is usually acquired with the same type of model (2-D or 3-D) as the one used within the reconstruction. Also, the electrode effects and the paracitics between cables are not accounted for. The latter constitutes the task of the second test.

b) *Laboratory or In-Vitro test.* Here, the imaging is carried out in the same way as the previous test, but the measured data comes from actual measurements performed on laboratory phantoms. This test is again established in two successive steps.

i) *Test with resistive network phantoms*. Depending on the case a 2-D or 3-D network is developed consisting of lumped resistors, which mimics a specific conductivity distribution. The measuring cables are directly (conductively) attached to the network periphery. The measured data include all the error-tolerances of the data collection system-hardware including the paracitics between the cables, but not the electrode effects.

ii) *Electrolyte Tank phantom*. This is a tank filled with an electrolyte solution (NaCl salt and water). Certain type of one or more cylindrical objects with conductivities different than the background are in turn introduced in the tank to serve as the target objects. The conductivity of the solution is controlled by the percentage of the salt solved in the distilled water. The electrodes are placed around the tank and are usually identical to those used for in-vivo measurements (Ag-AgCl type). This phantom includes all the effects occurring in the in-vivo measurements (the electrode contact impedance and its polarization are of primary importance), except the inaccuracy in the electrodes placement. Namely, the electrodes positions on the laboratory phantom are perfectly known.

c) *Clinical or in-vivo test.* This is the final stage and aims at the reconstruction of conductivity images from measurements on the actual human body. The major difficulty is the estimation of each electrode accurate position. This is critical, since a small error in the electrode position may cause significant deviation in the estimated (calculated) voltage. It is important for this test to have a means of measuring these positions accurately, in order for the computer model used in the reconstruction process, to accurately reflect the measurement topology.

4. DATA COLLECTION SYSTEM

The purpose of the data collection system is to apply different current patterns to the object to be imaged and to measure the developed voltage distribution on its surface. For this purpose, a number of electrodes is placed on its surface, a subset or even all of them are used to inject the low frequency current (usually 10 to 100KHz) and current amplitude less than 10mA. The measurement techniques can be generally discriminated in two - and four - electrode ones as shown in Fig.1.

For the two electrodes technique a constant current source is applied to the two electrodes and the voltage difference developed between them is measured, using these common leads. A serious problem occurs when voltage is measured across current carrying leads. Namely, the measured voltage (impedance) includes the effects of all the parasitic impedances appearing in series with the desired one. These include the switches/multiplexers resistance, the cables resistance as well as the electrode-object (skin) contact impedance. The latter one constitutes the actual problem, especially for measurements made on humans. The effects of all the others could be removed by proper calibration procedures, e.g. measuring a series of standard impedance connected at the electrode level. In contrary the electrode-skin contact impedance cannot be controlled or the contact is not repeatable and depends on the skin cleaning, the electrode material and the gel introduced between them to establish good electrical contact.

Due to the above problems the 4-electrodes technique is usually adopted and this is also done herein. For this one, two electrodes-cables (called ‘driven electrodes’) are used to inject the current, while two different ones (called ‘sensing electrodes’) are used for the measurement of the voltage differences. The input impedance of the voltmeter is very high (of the order of MΩ), since there is a differential (instrumentation) amplifier at the front end. Thus, the current flowing through the sensing electrode-cables is negligible (of the order of pA) and in turn the voltage drop on the parasitic series impedances is also negligible.

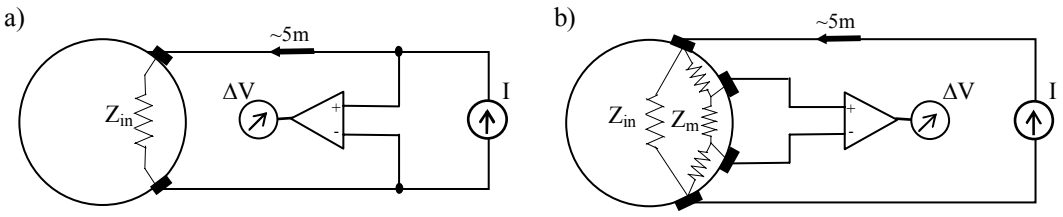

Figure 1. General principles of voltage-impedance measurement techniques in bio-impedance/EI applications, a) 2-electrode and b) 4-electrode techniques.

However, there is a number of proposed EIT techniques, e.g. Goble et al [8], that uses multiple electrodes to inject the so-called 'optimal current patterns'. Within that techniques it is impractical to avoid the voltage measurements on driven electrodes. For this reason they tried to model, the corresponding effects, e.g. Cheng et al, [9]. This technique may offer higher sensitivity but it increases the complexity in both the reconstruction algorithm and the electrodes. Also, the cost is so high that it may obscure all the EIT advantages over the classical imaging modalities. One could only consider the number of independent current sources required to see how the cost is increased.

The four electrodes technique is employed in the EIT system proposed herein as well as in our previous research. This decision has two major reasons, the simplicity and the lower cost. Moreover, the effort is directed toward the computer-laboratory and clinical test described in the introduction. Moreover, the best sensitivity achievable with one pair of driven electrodes studied in our previous work [3], is always adopted.

The purpose of the proposed data collection system is to support both 2 - as well as 3 - dimensional EIT imaging with the emphasis put toward the first two tests (computer and laboratory).

The placement of 16 electrodes around a circular and a rectangular object is shown in Fig.2 for the 2-dimensional imaging. Two of them must be driven, while the voltage differences between all the other pairs must be measured. When for example the current is injected through the electrodes 1-2, the voltage differences between the pairs 3-4, 4-5, . . ., 15-16 should be measured. This procedure constitutes one 'projection angle' in the classical imaging sense. The next pair of electrodes 2-3 is driven next and the voltage differences on all the other pairs are measured. This procedure continues until the measurements for all possible projection angles are collected.

Multiplexers are required in order to carry out the above procedure using a single current source and single "voltmeter". A convenient topology is shown in Fig.3, where a grid of 16×16 printed lines is formed.

The 16 ends of these lines are connected to each one of the 16×1 multiplexers. Each one of the horizontal lines is connected only with one of the vertical lines. Namely, only 16 nodes are created along one of the diagonal directions. Shielded coaxial cables are used to connect these nodes one-to-one with the electrodes placed around the object. In this manner each of the current source connector (+I, -I) or the voltmeter (+V, -V) can be connected to any one of the 16 electrodes.

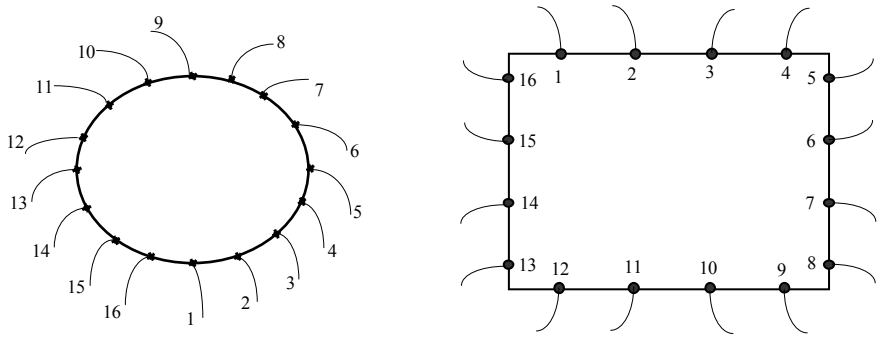

Figure 2. The equi-distance placement of 16 electrodes around a circular and a rectangular object.

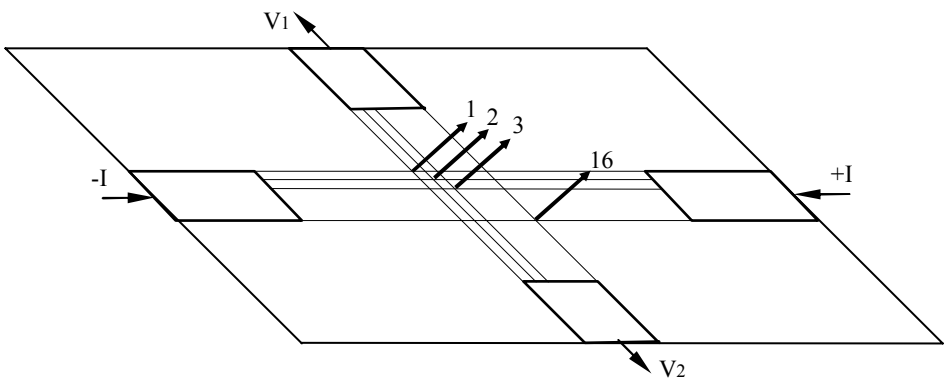

Figure 3. A four 16×1 multiplexer topology used to inject the current (+I, -I) at an electrode pair and to connect the voltmeter (+V, -V) at a different pair.

The placement of 64 electrodes on a 3-dimensional object is shown in Fig.4. These are arranged in four levels with 16 electrodes at each one of them. For each level the same interconnection (printed circuit) shown in Fig.3 is used, while an additional 4×1 multiplexer is used to connect these circuits to the source or the voltmeter.

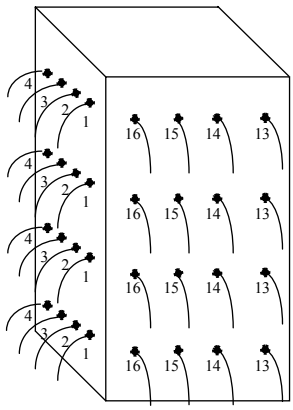

Figure 4. The placement of 4×16 electrodes around a three dimensional object

This is shown in Fig.5, which also presents the block diagram of he whole data collection system. Alternatively, a different "voltmeter" can be used for each level to increase the speed of the data collection. This topology can be extended to more levels if required.

The term "voltmeter" is used in the above description, but in fact an analog-to-digital converter (A/D) in conjunction with a sample and hold (S&H) circuit is used instead

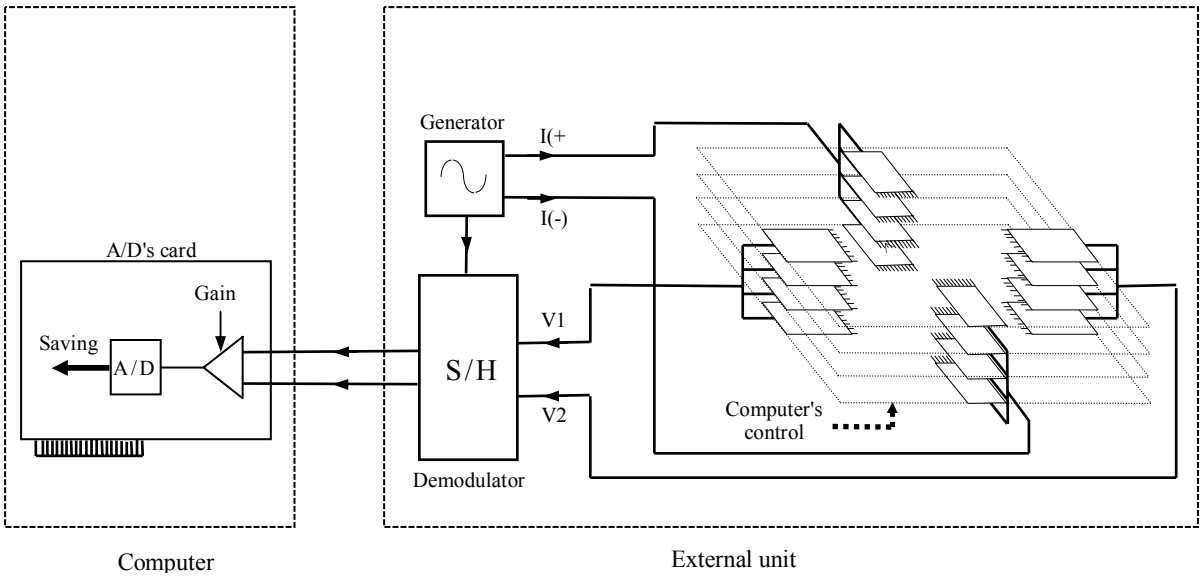

Figure 5. Block diagram of the whole data collection system.

At this point the important subject of the demodulation must be clarified. As described before a sinusoidal constant current is injected to the object to be imaged. But the object in general and especially the human tissues behavior is not purely resistive. This is due to the fact that apart of their conductivity they have a dielectric constant very much different than that of the air. For example the blood at 50 KHz has ε_r= 150. As explained in one of our

works, Sahalos et al [5], in a purely resistive object (σ, ε_r=1) the developed voltage differences are in-phase with the injected current waveform. In contrary in a perfect dielectric object (σ=0, ε_r>1) the developed voltage will be exactly out-of-phase (90^0 phase difference or a quarter of the period shift in time). Likewise, in the general case the voltage will have an arbitrary phase shift, but this can be analyzed into two components, one in-phase and another one out-of phase. This is easily understood when the complex phasors definition is used. The question is how to measure these two components separately. This is a very well known issue in communications and it is solved employing "synchronous demodulation". Namely, the in-phase component is obtained by multiplying the voltage to be measured by the source waveform, while the out-of-phase is obtained when this voltage is multiplied by a replica of the source waveform shifted by 90^0. Instead of the classical synchronous demodulation technique its implementation using “digital sampling” is more compatible with EIT data collection as explained by Koukourlis et al [12]. This is shown in Fig.6, where the source (injected current) and the voltage waveforms are shown along with in-phase and out-of-phase pulse trains. A digitally synthesized sinewave generator is employed for the current source, [5, p.243]. The sinewave samples (64 or 128) are stored in an EPROM, which is sweep by a counter at a sufficient rate depending on the desired frequency. The digital samples are fed to a digital to analog converter (DAC) and then to a voltage to current circuit. For more details on can contact [5, p.243] and the references therein. The important advantage of the digitally synthesized source is the ability to provide us with the synchronization pulse trains (Fig.6) at the maximum and zero crossing of the sinusoid. These pulse trains are used to trigger the S&H circuit as shown in Fig.5. This in turn holds a dc-voltage value fed to the D/A converter until the conversion is finished.

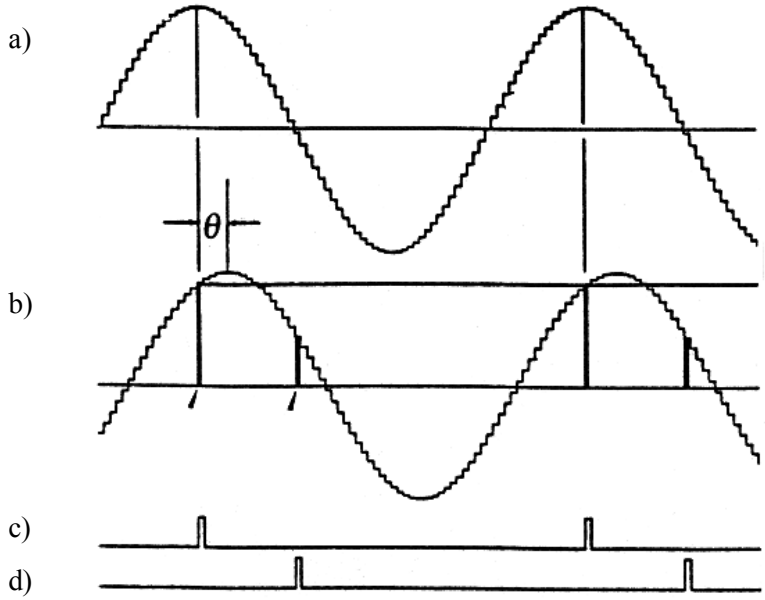

Figure 6. Example of the waveforms for a) the constant current source and b) voltage to be measured. The in-phase c) and out-of-phase d) pulse trains provided by the source are also shown.

Commercial boards for the A/D and S&H units are used in the present implementation, while the source, the multiplexer and all the supporting circuits are locally designed and fabricated. Specifically the National Instruments AT-MIO-16XE50 A/D board with 16bit resolution and 20KHz maximum sampling rate is used. This board includes an externally triggered S&H circuit, but the simultaneous S&H board of the same company is used instead. This configuration offers several advantages. First, the S&H circuit is placed in the multiplexers unit (outside the computer) and includes amplifiers (used as preamplifiers). But more important the SC2040 offers a simultaneous S&H option on 8 differential channels. This option can be used to increase the data collection speed preserving the same phase among channels. A new system is already under development using two simultaneous S&H boards with all 2×16 (+V, -V) lines of Fig.2 directly connected on their 16 differential channels. This is important for the in-vivo measurements where the cardiac signals should be excluded from the measured values.

Another issue not mentioned above is the parasitic capacitance occurring between the cables. These effects cannot be avoided by the 4-electrode technique, but these capacitances contribute only to the out-of-phase (imaginary) component of the measured voltage. Thus, it presents a problem to the dielectric constant imaging, but not to the conductivity imaging in which we are presently interested.

Concerning the shielded coaxial cables used to connect the electrodes with the multiplexers unit, care must be taken to avoid possible ground loops [13]. The recommended practice for low frequencies is to connect the cables outer conductor only at one point, preferably at the 'source' side. Where as 'source' side is assumed the point where the voltage to be measured is generated, namely near the electrodes. But, this is practically inconvenient. Thus, all the coaxial cables outer conductors (shields) are connected together and are grounded only at the multiplexers unit.

Finally, another important issue is the necessity of DC-block capacitors between the electrodes and the S&H terminals. Irrespective whether the measurements are made on a tank containing an electrolyte or on human tissue (the body fluids are also electrolytes) a DC voltage is developed on the electrode. This is due to the exchange of ions or electrons between the electrode and the electrolyte. This phenomenon is uncontrollable, it is affected by the temperature and it can result in arbitrary DC voltages on each electrode in the range of about -1.66V to 1.69V, [14, p.243]. The block capacitor value is critical. A large capacitance value serves the insertion of a low value series resistance. But since the input impedance of the instrumentation amplifier that follows is very high (of the order of 100MΩ) then the capacitor loading time becomes large. This would lead to a degradation of the data collection speed. So, a practical compromise is always adopted.

5. RECONSTRUCTION ALGORITHM

The reconstruction algorithm aims at the estimation of the internal conductivity distribution based on the measured voltage data set and a corresponding calculated one. A detailed description of the measurements set-up is given in the previous section. As explained before the calculated voltage data set is obtained from the solution of the generalized Laplace equation (1), for each one of the injected current patterns considering an initial-starting conductivity distribution. This is usually a homogeneous one with a value preferably equal to a guess for the object's average conductivity. In the tank case the starting value is estimated from the amount of salt solved in its distilled water content. For more complicated objects, like the human thorax, any a priori known information should be used. A physiological subject model using the already known average values for each tissue, Geddes and Baker [15], is considered a very good starting distribution. Since, the primary application interest in EIT is the continuous patient monitoring, it was suggested that the exact body internal and peripheral structure could be obtained from an MRI or CT

image (these are performed only once). This approach could also be of primary importance for the estimation of the exact electrodes positions.

Returning back to the solution of the forward problem, its fast and accurate solution determines the speed of the reconstruction since multiple (equal to the number of projection angles) forward solutions are required for each iteration of the inverse problem. A piecewise constant conductivity distribution in conjunction with the Finite Element Method (FEM) is best suited for the EIT problem. The solution domain is subdivided into small elements which are identified as the pixels (for 2-D) or the voxels (3-D) of the image. The conductivity within each element is assumed homogeneous but its value is in general different for each element. The smaller these elements are the better the method spatial resolution. But, the number of the elements cannot be greater than the number of available linearly independent measurements (this will be explained latter).

The boundary conditions to be imposed on Eq.(1) include the applied current on each electrode and the continuity conditions at the interelement interface and the object-air interface. These are as follows:

$$-\sigma\frac{\partial V}{\partial n}=\begin{cases}\text{J on the electrodes}\\ \text{0 at the body - air interface}\end{cases} \tag{2a}$$

where $\partial V/\partial n$ is the potential derivative normal to the surface

At the elements (i,j) interface it is:

$$V_i = V_j \text{ and } \sigma_i\frac{\partial V}{\partial n_i}=\sigma_j\frac{\partial V}{\partial n_j}. \tag{2b}$$

With the aid of the variational principle the generalized Laplace equation (1) along with the boundary conditions is reduced to the minimization of the functional:

$$F(V)=\frac{1}{2}\iiint_{V_D}\left\{\sigma_x\left(\frac{\partial V}{\partial x}\right)^2+\sigma_y\left(\frac{\partial V}{\partial y}\right)^2+\sigma_z\left(\frac{\partial V}{\partial z}\right)^2\right\}dxdydz+\oiint_S JVdS \tag{3}$$

where S is the electrodes surface and V_D is the solution volume.

Employing the superposition principle the integral of Eq.(3) is performed over each element volume separately. Moreover, in order for F(V) to be minimized its partial derivatives with respect to each element nodes should be set to zero, as:

$$\frac{\partial F(V)}{\partial V_i}=0 \text{ for } i=1, 2, \ldots, N_p \tag{4}$$

where N_p is the number of nodes.

All the necessary details for the application of FEM can be found in our previous works, e.g. [5], [6] and [10]. Summarizing herein, a bilinear (2-D) or trilinear (3-D) interpolation function is assumed for the unknown potential V(x,y,z) within each element. Its number of unknown constants is equal to the number of the element nodes (on its vertexes). Applying V(x,y,z) on all the nodes (with potential V_i) and solving the resulting system for these unknown constants, V(x,y,z) is expressed in terms of the nodal voltages V_i. In turn the derivatives and integrations involved in equations (3) and (4) are analytically performed resulting in a system of equations for each element of the form:

$$[Y^e][V^e]=[I^e] \tag{5}$$

Where $[Y^e]$ is an admittance matrix, $[V^e]$ the unknown nodal voltages and $[I^e]$ the current injected in each node. The latter is zero on most of the nodes except the ones constituting the metallic driven electrodes. Recalling then that, all the internal nodes will be shared among multiple elements (4 for 2-D rectangular grid and 8 for a 3-D one), then each nodal-voltage should be enforced to be identical in all these elements. This consideration results to a procedure known as "Master Matrix Assembly". Namely, all the element equations (or matrices) are summed together but keeping in mind which nodal voltages should be identical (details in [5, 6, 10]). The final linear system of equation is similar to that of Eq.(5) but for the whole object:

$$[Y][V]=[I]. \tag{6}$$

Several techniques can be employed for the solution of (6), among them is the Gauss Jordan elimination, the LU decomposition and the Gauss Seidel iterative scheme. Since, the inverse problem involves multiple iterations requiring the solution of (6) on models with the same excitation and small differences in the conductivity distribution we chose to use the Gauss Seidel scheme. Within this, the solution of the first inverse problem iteration are used as starting-guess for the corresponding ones of the next iteration. Especially for the 3-D case this approach minimizes the memory and CPU time requirements. However, within the same inverse problem iteration the required solutions involves the same matrix $[Y]$ with different right hand sides $[I]$. This justifies the approach of evaluating first the inverse matrix $[Y]^{-1}$ and calculating then the multiple solutions by simple multiplications. This is in turn in favor of choosing the LU decomposition, which is the most robust and stable technique. However, for a large number of nodes (e.g. 3-D problems) the total speed is in favor of iterative schemes. Thus the final choice is problem dependent. The Gauss-Seidel iterative scheme modified to include a relaxation factor K is as follows:

$$\left.\begin{aligned} V_i^n &= V_i^{n-1} + k\cdot\left(\tilde{V}_i^n - V_i^{n-1}\right) \\ \tilde{V}_i^n &= \left\{ I_i - \sum_{\ell=1}^{26} Y_{i\ell} V_\ell^m \right\} \Big/ Y_{i1} \end{aligned}\right\} \tag{12}$$

where l = NEBOR(j,i) = global number of the j-th neighboring node to the i-th node-line currently processed. Y_{i1} is the coefficient of V_i itself and V_ℓ^m the voltage of the l-th node, some of which are updated at the current (n) and some in the previous (n-1) iteration.

The algorithm starts from an initial solution $[V]^o$ and all nodal voltages are updated at each iteration. This is iteratively repeated until the maximum voltage change, (error) at any node, between successive iterations becomes less than a prespecified error tolerance (e.g. 10^{-6}). The relaxation factor value is in general between 0 and 2. For the solution of Laplace equation we found that the optimum value giving the fastest convergence is k=1.75.

A reconstruction algorithm named "Modified Perturbation Method" was developed in our previous work [10] and was latter extended to 3-D imaging [6]. This has the form:

$$\sigma_j^n = \sigma_j^{n-1} + k\frac{\sum_{i=1}^{M} \frac{V_{mi} - V_{ci}}{V_{mi}} \frac{\partial V_i}{\partial \sigma_j}}{\sum_{k=1}^{M} \left| \frac{\partial V_k}{\partial \sigma_j} \right|} \sigma_j^{n-1} \tag{13}$$

where the superscript n denotes the iteration and M is the total number of linearly independent measurements from all projection angles (driven electrodes combinations). V_{mi} and V_{ci} are measured and calculated voltage differences at the i-th sensing port. K is again a relaxation factor. Until now we have set k=1, since a higher or lower value does not seems to improve convergence. The derivatives $\partial V_i / \partial \sigma_j = J_{ij}$ are elements of the "Jacobian matrix" and they express the sensitivity of the i-th pair (-port) of voltage sensing electrodes to the changes of the j-th pixel conductivity. The Jacobian matrix is given by a closed form expression, which is developed, based on the "Electric circuits compensation theorem" for both 2-D and 3-D geometries, [6,10]. The same formula applies for both cases and it is:

$$J_{ij}(\sigma) = \frac{\partial V_i}{\partial \sigma_j} = -\frac{1}{I}\sum_{\ell=1}^{L} S_\ell \, V_{ij(\ell)} \cdot V_{kj(\ell)} \tag{14}$$

where L is the total number of resistors forming the i-th element (L=6 for 2-D and L=28 for 3-D elements). Namely, the non-diagonal components of each FEM element matrix $[Y^e]$, like that of Eq.(5) define a resistor network and the conductance of the l-branch is

$Y_\ell^e = S_\ell \cdot \sigma_j$. Thus, the coefficients S_l are defined by the non-diagonal components of the element matrix $\left[Y^e\right]$. The voltage differences $V_{ij(l)}$, $V_{kj(l)}$ are developed along the l-th resistor when the driven pair of electrodes (-port) is respectively the i-th and k-th. These voltage differences are directly calculated from the nodal voltages obtained from the solution of Laplace equation for each projection angle. It must be noted that the same solutions are used to estimate the calculated voltages on the electrodes. What is additionally needed to evaluate the Jacobian $\left[J_{ij}\right]$ is to store the nodal-voltages for all the solutions.

6. NUMERICAL RESULTS AND DISCUSSIONS

One of the first tasks was the validation of the quasistatic approximation and the Finite Element modeling. For this purpose an 8×8 elements (Fig.7a) computer phantom was simulated using both FEM and a circuit analysis software (HP-MDS: microwave design program). The former (FEM) performs a DC analysis while the latter performs an AC analysis. The equivalent circuit for each element result from the non-diagonal coefficients of the element-matrix. When the material is assumed purely resistive a resistive network is obtained (Fig.7b) while when the displacement current effects are included a capacitance related to the dielectric constant is added parallel to each resistor (Fig.7c). For the resistive network, where the quasistatic approach is absolutely valid, the FEM and MDS results are found to be identical to the 4th decimal digit, (the FEM system is solved with a 10^{-6} tolerance). The limits of the quasistatic approach are defined in Fig.8a, where the AC simulation results from the resistive and the R//C networks are compared. Considering an acceptable error of the order of 0.1 %, Fig.8b shows that the quasistatic approximation can be safely used upto about 2.8 MHz.

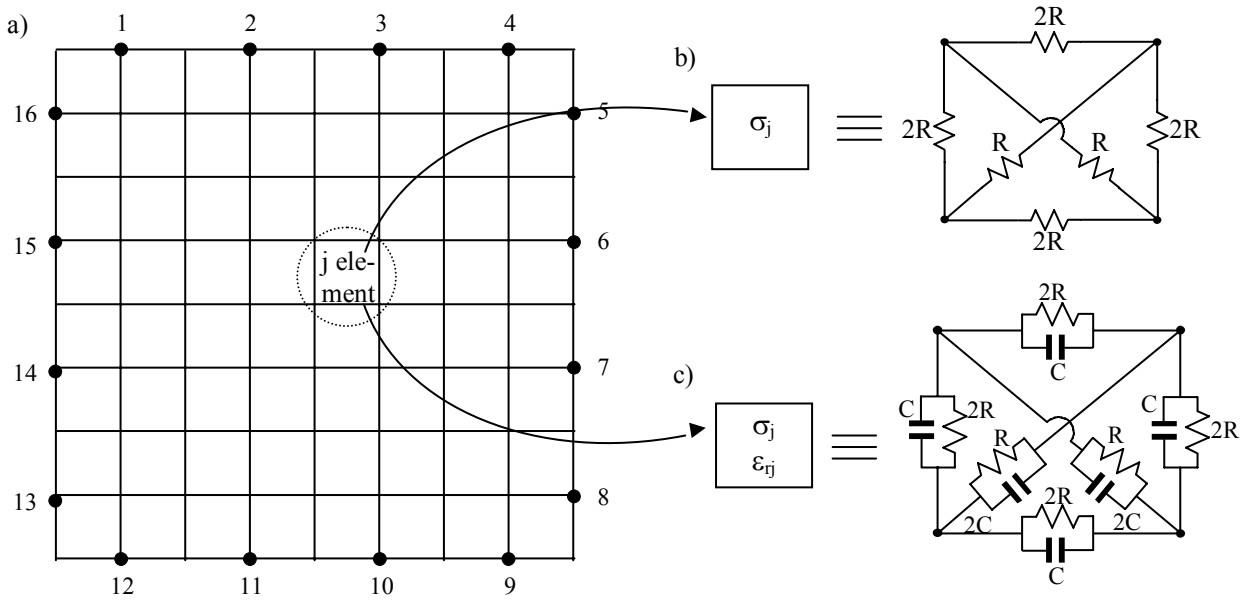

Figure 7. a) An 8×8 element FEM model which is either b) purely resistive (conductive material $\sigma \rightarrow R=3/\sigma_j$) and c) lossy dielectric material ($R=3/\sigma_j$ and $c=\varepsilon_o\varepsilon_{rj}/6$). It is assumed that σ_j = 7.69 mS/cm, ε_{rj} = 150 and ε_o = $8.854 \cdot 10^{-12}$ F/m.

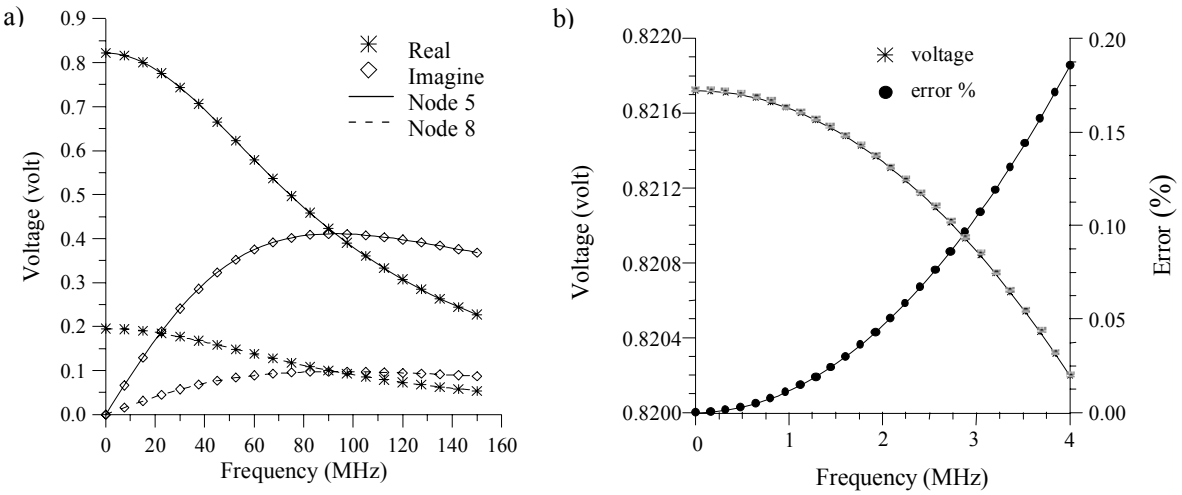

Figure 8. a) Voltage difference at an electrode pair versus frequency for two cases of Fig.7, b) voltage and error variation of node 5 for the model of Fig.7 versus frequency.

The first laboratory phantom considered was the resistive network (using surface mount resistors) shown in Fig.9. Some selective sub-areas of this network are left blank and the sub-networks shown on the left of Fig.9 can be inserted there. In this manner, either a homogeneous model or a model including one or more conductivity "anomalies" can be realized. A comparison between the FEM model results and the measurements on the

resistive network, for both a homogenous phantom and one with a simple anomaly are shown in Fig.10. The very good agreement shown in Fig.10 is also observed for all the cases examined.

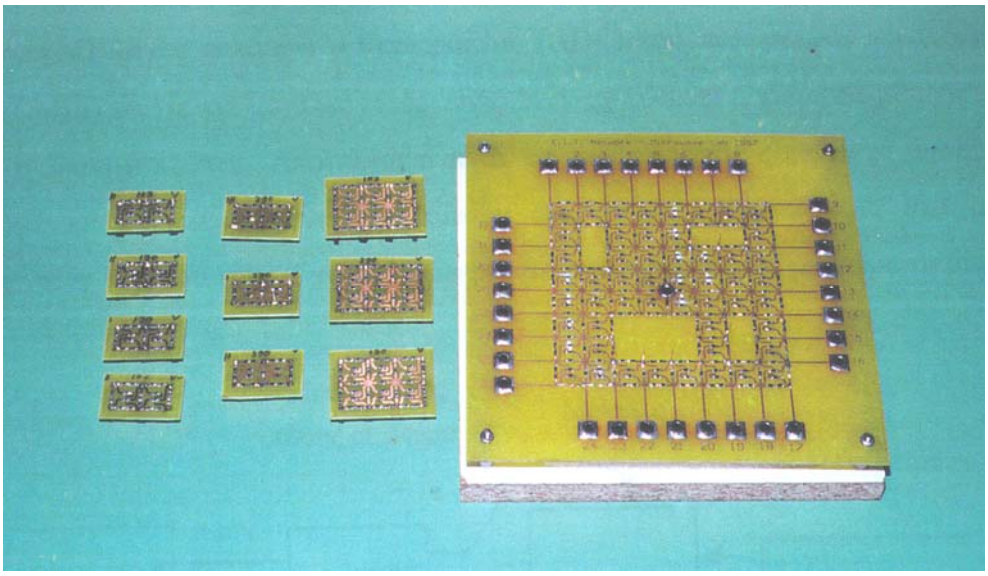

Figure 9. Photograph of the resistor network laboratory phantom with 16 electrodes on the outer periphery. The sub-networks shown on the left are in turn attached at the empty area of the model.

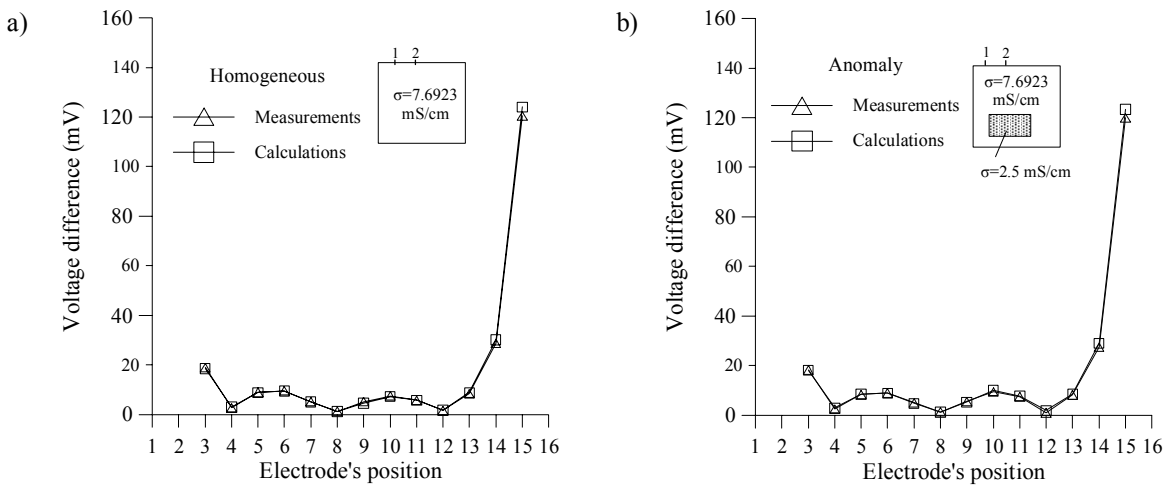

Figure 10. Comparison of results from the resistive network laboratory phantom and a FEM model, a) for a homogeneous and b) for a phantom with a single anomaly.

A resistive laboratory phantom with an anomaly of higher conductivity, in respect to its homogeneous background (obtained by introducing the corresponding "lower" resistance sub-network into the network of Fig.9), is then measured as explained in section IV. The collected measured data set is in turn used from the 2-D MPM reconstruction algorithm, where a homogeneous starting solution is assumed. The same procedure is repeated for a "lower" conductivity (higher resistances) laboratory phantom. The results are shown in

Fig.11 where the reconstructed images are compared against the "assumed" target phantoms. It can be seen that the EIT process clearly identifies the position and the conductivity of the anomaly. But, as observed in the computer phantom-test [10] and it is the characteristic of any EIT-technique, the image can not follow the step change in the conductivities and it rather gives a smooth change.

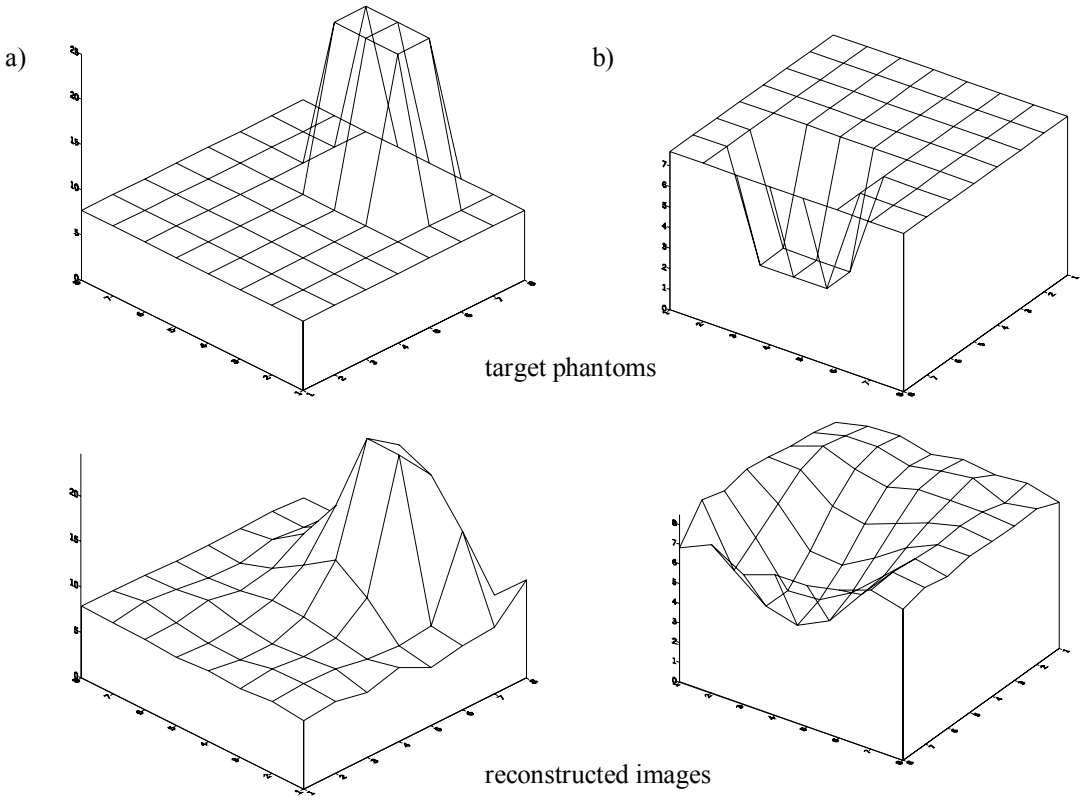

Figure 11. Conductivity images reconstructed from a resistive laboratory phantom (Fig.9) compared against the assumed target phantom, a) for higher conductivity and b) for lower conductivity single anomaly at the 8th and 6th iteration respectively.

As explained in the theoretical part, the resistors-network phantom does not include the electrode polarization and contact impedance effects. For this purpose we developed the tank laboratory phantom shown in Fig.12a which has 16 electrodes on its mid-level. A similar one with electrodes at 4-levels (Fig.12b) is also developed in order to test the 3-D algorithm (this is currently undertaken). Block capacitors are also included in series with the electrodes to cut-off the electrodes polarization effects, as explained in section IV. Two rectangular cylinders a metallic ($\sigma \rightarrow \infty$) and a plastic ($\sigma$=0) are used as target anomalies.

a}

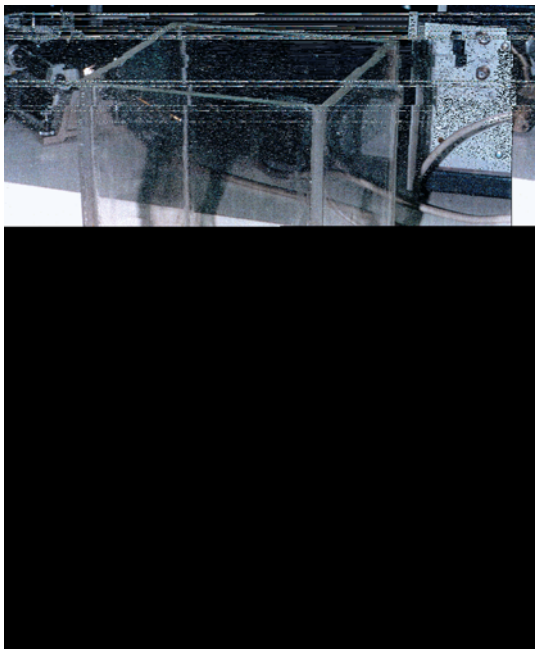

b}

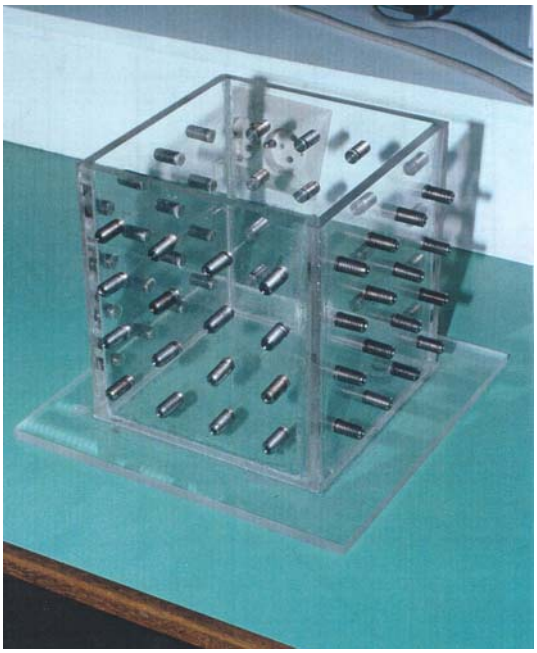

Figure 12 a) Photograph of the tank with 16 electrodes, and b) the tank with 4×16 electrodes.

Reconstructions are for the time being available only for the phantom of Fig.12a. The measured data set is collected in the usual manner. A FEM simulation is then performed both for a 2-D model (cross-section at the electrodes plane) as well a 3-D complete model. The comparison of the measured results and the two simulated ones is shown in Fig.13. Notice that results at the driven electrodes and at the ones next to them are not presented, since the 4-electrodes technique is employed. In fact, what Fig.13 shows is the voltage difference between neighboring electrodes, which constitutes the actual information. A fairly good agreement between the measurements and the 3-D simulated data is observed. But, the 2-D simulated data are quite larger. A closer examination shows that these are actually a magnification of the measurements. This is simply due to the fact that in the 2-D model all the current is forced to flow in a single plane. Two alternative approaches are used to face this problem. The first one and the more general is to employ the 2-D reconstruction algorithm but calculate the necessary voltages from a 3-D FEM model. The second approach is to use a purely 2-D imaging but employing a reduced magnitude of the injected current in the calculations. The reduction ratio is estimated as the mean value of the ratio of the calculated voltage differences (with the same current) over the measured

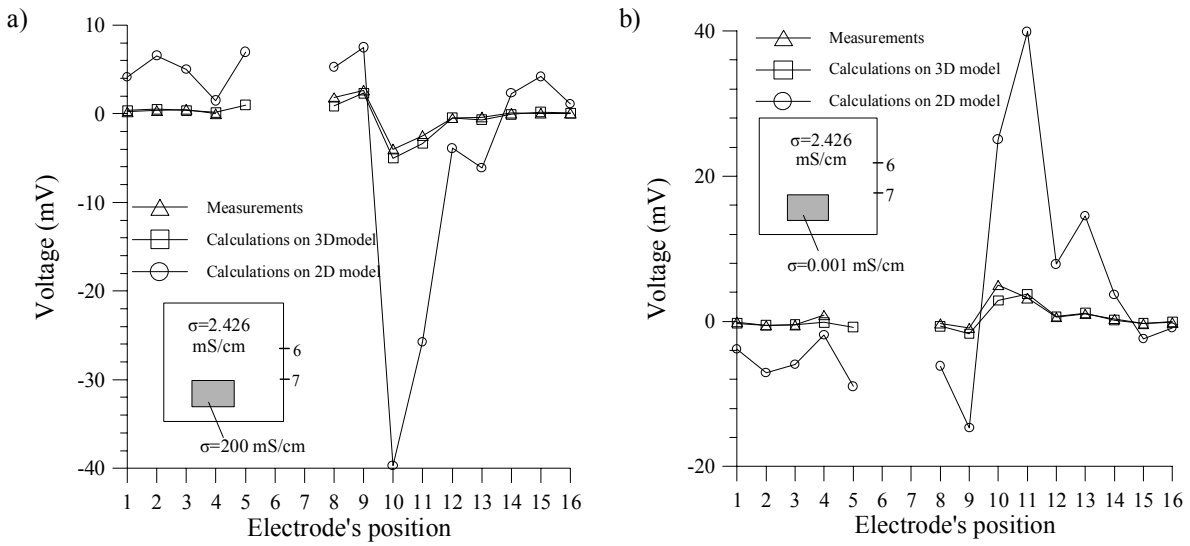

Figure 13. Comparison of the measurements on a tank filled with an electrolyte solution and the simulated ones from a 2-D and 3-D FEM model, a) for a metallic and b) for a plastic anomaly.

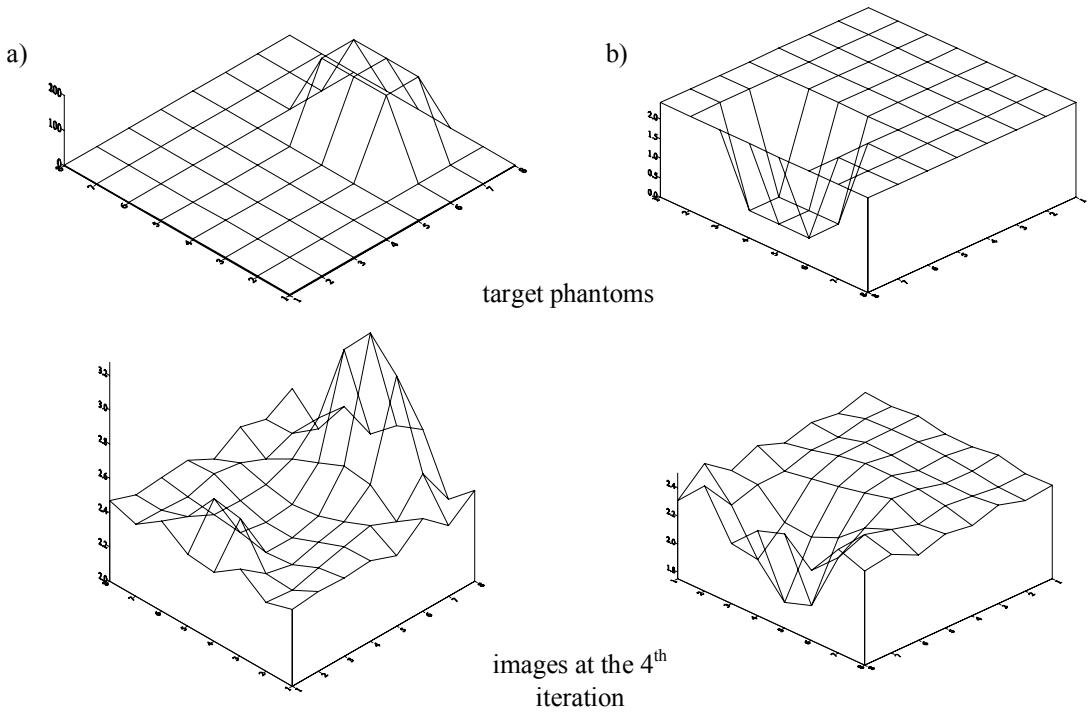

Figure 14. Conductivity images reconstructed from a tank containing electrolyte solution at the 4th iteration, a) for a metallic and b) for a plastic anomaly.

ones. The latter approach is only for testing purposes and it does not seem to be general. A more substantial solution is to employ a full 3-D EIT imaging, which in turn requires electrodes at multiple levels.

The conductivity images obtained at the 4th iteration from the 2-D reconstruction algorithm and the measurements on the phantom of Fig.12a are shown in Fig.14. These are also compared against the "assumed" target model. The position of the anomaly is fairly good identified, but some minor artefacts are also occurring.

7. CONCLUSIONS

The step-by-step procedure followed for the development of our EIT system is presented. This includes both the hardware or data collection system and the software, namely the reconstruction algorithm. This work can serve as a guide for anyone who would like to develop his own EIT system. Laboratory phantoms are developed and tested. The corresponding images observed appears to be very promising for the next phase of this research, which is the "in-vivo" testing of the system. Finally, the 3-D reconstruction seems to be the most appropriate technique and its laboratory test is already undertaken.

REFERENCES

[1] D.C. Barber and B.H. Brown, “Applied potential tomography”, J. Phys. E. Sci. Instrum., vol.17, pp.723-733, 1984.

[2] K.A. Dines and R.J. Lytle “Analysis of Electrical Conductivity Imaging”, Geophysics, vol.46, pp.1025-1036, 1981.

[3] R. Hauf, “Effects of current passing through the human body, Revision of IEC publication 479”, International union of Electrotechnical Comission, 1984.

[4] B.H. Brown, “Tissue Impedance Methods”, in “Imaging with non-ionizing radiations” edited by Daphne F. Jackson, Survey Univ. Pres., 1983.

[5] J.N. Sahalos, G.A. Kyriacou and C.S. Koukourlis, “Techniques in Electrical Impedance Tomography (EIT)”, vol.5: Modalities appearing as chapt.5 in “Medical Imaging Systems and Applications” edited by C.T. Leondes, Gordon and Breach SC Pub., Amsterdam 1997.

[6] G.A. Kyriacou, C.S. Koukourlis, P. Bonovas and J.N. Sahalos, “A reconstruction algorithm for the three dimensional Electrical Impedance Tomography”, BSUAE J. of Applied Electromagnetism, vol.1, no.1, pp.13-36, Oct. 1997.

[7] G.A. Kyriacou, P. Bonovas, C.S. Koukourlis and J.N. Sahalos, “Electrical Impedance Tomography System and Reconstruction Algorithm”, PENED 1995/1811, project financed by GSRT (General Secretariat of Research and Technology-Greece”, Demokritos Univ. of Thrace, Xanthi 1999.

[8] J. Goble and D. Isaacson, “Optimal current patterns for three-dimensional computed tomography”, Proc. Annual Int. Conf. IEEE Eng. in Medicine and Biology Soc., vol. 11., pp. 463-464, 1989.

[9] K.S. Cheng, D. Isaacson, J.C. Newell and D.G. Gisser, “Electrode models for

electric current computed tomography", IEEE Trans., Biom. Eng., BME-36, pp.918-924, 1989.

[10] G.A. Kyriacou, C.S. Koukourlis and J.N. Sahalos, "A reconstruction algorithm of electrical impedance tomography with optimal configuration of the driven electrodes", IEEE Trans. on Medical Imaging MI-12, no.3, pp.430-438, Sept. 1993.

[11] C.S. Koukourlis, G.A. Kyriacou and J.N. Sahalos, "A 32 electrode data collection system for electrical impedance tomography", IEEE Trans. on Biomedical Engineering, vol. 14, pp.630-636, June 1995.

[12] C.S.Koukourlis, G.A. Kyriacou and J.N. Sahalos, "Differential synchronous demodulation for electrical impedance tomography", Clin. Phys. Physiol. Meas., Vol. 13, Suppl. A, pp. 31-34, 1992.

[13] HP-Application Note 123: "Floating Measurements and Guarding", Palo Alto, CA, 1983.

[14] M.E. Valentinuzzi, "Bioelectric Impedance Techniques in Medicine", in "Critical reviews in Biomedical Engineering", editor J.A. Bourne, Begell House, vol.24, Issues 4-6, 1996.

[15] Geddes L.A. and Baker L.E., 1967, "The specific resistance of biological material – A compendium of data for biological engineer and physiologist", Med. Biol. Eng., Vol. 5, pp. 271-293.

Acknowledgments: The authors would like to thank the General Secretariat for Research and Technology of Greece (G.S.R.T.) who has partly financed the present research effort.